In Situ Tracking of Ion Insertion in Iron Phosphate Olivine Electrodes via Electrochemical Quartz Crystal Admittance

ARTICLE *in* THE JOURNAL OF PHYSICAL CHEMISTRY C · JANUARY 2013

Impact Factor: 4.77 · DOI: 10.1021/jp3117819

7 AUTHORS, INCLUDING:

Levi Mikhael
Bar Ilan University
193 PUBLICATIONS **8,746** CITATIONS
SEE PROFILE

Sergey Sigalov
Bar Ilan University
13 PUBLICATIONS **187** CITATIONS
SEE PROFILE

Ran Elazari
Israel Chemicals Limited
18 PUBLICATIONS **1,768** CITATIONS
SEE PROFILE

Leonid I Daikhin
Tel Aviv University
65 PUBLICATIONS **1,348** CITATIONS
SEE PROFILE

THE JOURNAL OF PHYSICAL CHEMISTRY C

Article

pubs.acs.org/JPCC

In Situ Tracking of Ion Insertion in Iron Phosphate Olivine Electrodes via Electrochemical Quartz Crystal Admittance

Mikhael D. Levi,*[,†] Sergey Sigalov,[†] Gregory Salitra,[†] Ran Elazari,[†] Doron Aurbach,*[,†] Leonid Daikhin,[‡] and Volker Presser[§]

[†]Department of Chemistry, Bar-Ilan University, Ramat-Gan 52900, Israel

[‡]School of Chemistry, Raymond and Beverly Sackler Faculty of Exact Sciences, Tel-Aviv University, Ramat Aviv, 69978, Israel

[§]INM – Leibniz-Institute for New Materials, D-66123 Saarbrücken, Germany

Supporting Information

ABSTRACT: $LiFePO_4$ is one of most promising cathode materials for lithium-ion batteries (LIBs) due to its superior rate handling ability, moderate cost, low environmental hazards, and safe long-term cyclability. In addition to the electrochemical information on the charge and discharge process, electrochemical quartz crystal admittance (EQCA) of LIB electrodes provides direct access to potential-driven frequency shifts (Δf_{exp}) and changes of the resonance peak width ($\Delta\Gamma$) due to Li-ions insertion/extraction. It is not only possible to monitor mass changes of the electrode, but the two parameters Δf_{exp} and $\Delta\Gamma$ also reflect mechano-structural changes caused by hydrodynamic solid–liquid interactions from the operation of a LIB. Applying a suitable model that takes into account such interactions, potential-induced changes of the effective thickness and permeability of the composite electrode have been determined. The latter shows that ion insertion/extraction results in a nonuniform deformation of the electrode. Using EQCA as a unique mechanical probe for insertion-type electrodes, the dynamic effect of the local host environment on Na^+-ions insertion/extraction has been studied in a mixed solution of Li- and Na-salts. As a highly reliable and quantitative tool, EQCA may enable a broader understanding of coupled electrochemical and mechanical events in LIB during their long-term operation. This includes information about the distortion/deformation of the electrode intercalation particles and the entire composite electrode under polarization. Also, EQCA can help to clarify the role of polymeric binder in the composite electrodes as the factor stabilizing long-term cyclability of Li-ions batteries.

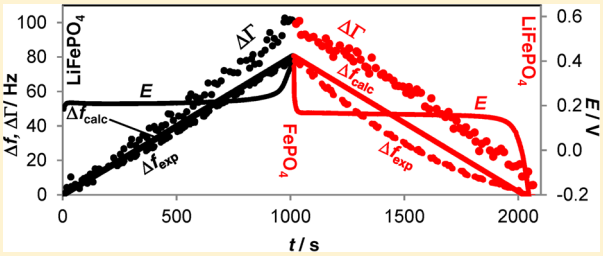

1. INTRODUCTION

Recently, lithium-ion phosphate ($LiFePO_4$) has emerged as a particular attractive cathode material for high power Li-ion batteries (LIB).[1a] An extremely narrow range of solid solutions between the two end-members $LiFePO_4$ and $FePO_4$ creates a driving force for a highly anisotropic first-order phase transition during electrochemical insertion/extraction of Li-ions.[1b] The large crystallographic mismatch between the frameworks of Li_1FePO_4 and Li_0FePO_4 can induce considerable host volume changes up to 6.5 vol %, inducing significant stress in the electrode particles.[2] This stress can be detrimental to both the rate handling ability and the cycling life of a battery.[3] For example, stress relaxation easily results in mechanical degradation of the electrode coating and premature device failure.[4] For an improved understanding of the underpinning effects and for an optimized application in LIBs, we need to utilize reliable and quantitative methods for an extended in situ investigation of distortion/deformation of the composite electrode layer upon Li-ions insertion/extraction. The latter causes volume changes, which lead to the buildup of stress and strain in a composite electrode in a very complicated manner because of nonuniformity of the porous composite electrodes' structure. The simplest case consists of a homogeneous, nonporous active mass layer, which is clamped from one side and free on the other, that is, a layer that is attached rigidly to a Si wafer or to a quartz crystal surface and is open for ion insertion/extraction on the side facing the bulk solution. In that case, conventional probe-beam deflection[5a] or an advanced multibeam optical sensor wafer-curvature system[5b−e] can be used for direct determination of stress by monitoring the extent and sign of the curvature of the electrode coating on a glass substrate or Si-wafer, respectively. If the electrode's active mass is deposited onto the surface as a porous layer with the pores filled with the electrolyte solution and if the layer has a constant thickness, the system is becoming very complicated, and the measured stress starts to be dependent on the detailed structure of the porous electrode. In the present case, we have to consider a two-phase system: the solid phase as a matrix with a liquid inside its porous body. It is now easy to realize that the conventional composite electrode accounting for at least four

Received: November 30, 2012
Revised: January 1, 2013
Published: January 2, 2013

   dx.doi.org/10.1021/jp3117819 | J. Phys. Chem. C 2013, 117, 1247−1256

simultaneously present phases (solid intercalation particles, solid carbon black conductive additive, rigid/viscoelastic polymeric binder, Li^+-ion containing electrolyte solution) may demonstrate a much more complicated mechanical response upon ions insertion/extraction as compared to that for a porous but macroscopically uniform film electrode. The situation with practical composite electrodes used in Li batteries is even more engrafted by a broad intercalation particles size distribution and macroscopically different effective thicknesses of the electrode coatings. A question arises whether the mechanical changes in charged electrodes with a complicated porous structure can be reliably measured, theoretically interpreted, and finally used for the prediction of Li-batteries cycling life.

This Article investigates the ways in which in situ electrochemical quartz crystal admittance (EQCA) may contribute to solve critically important problems related to composite electrodes in Li-ion batteries. EQCA is a three-channel data acquisition method that provides direct access to the resonance peak width of the electrode coating, Γ, in addition to the intercalation charge, Q, and the resonance frequency shift, Δf_{exp}.[6] This method has been technically well advanced during the last two decades and successfully used for studying a variety of the processes occurring with coated quartz crystals in different media, such as adsorption of species from gaseous and liquid phase, films swelling, or crystalline-to-amorphous phase transition.[6] This study is not the right place to refer to a vast literature devoted to technical advancement of this technique; we can only mention recent reviews on this issue. However, outstanding contribution to the establishment and practical use of this technique should be specially acknowledged by several groups[7] and is documented in some reviews.[6b,c] Full QCA analysis of the electrochemical processes has also been carried out for the redox- and electronically conducting polymers.[8a] So far, Li-batteries electrodes have been studied only as binder-free vacuum deposited films,[8b] or prepared by spray pyrolysis.[8c] However, this was done by a two-channel EQCM technique, which is suitable to trace mass changes in the electrode coatings rather than potential-induced mechanical changes. As far as we know, composite electrode materials for Li-ion batteries have not ever been characterized even by a simple EQCM technique.

In this work, we apply, to the best of our knowledge for the first time, the EQCA technique to measure full quartz-crystal admittance of composite $LiFePO_4$ electrodes. This allows us to experimentally determine the change in the resonance frequency shift Δf_{exp} as well as in the resonance peak width $\Delta\Gamma$, characterizing oscillation energy dissipation in the composite electrode due to distortion/deformation of the active (intercalation) particles and their hydrodynamic interaction with the contacting electrolyte solution. A recently reported hydrodynamic model of such interactions[9] has been applied, and it reveals a complicated nonuniform character of the potential-dependent deformations of the intercalation particles. These interactions were shown to be dependent on the nature of the solvent and the binder, implying the ability of EQCA to reflect in situ the mechanical status of cycled composite electrodes.

Recently, the focus of battery research has strongly advanced beyond the scope of pure lithium intercalation, and significant research activities are now focused on Na-ion batteries.[10] In our study, we adapted in situ EQCA for studying the process of insertion/extraction of Li^+- and Na^+-ions in the composite Li_xFePO_4 or Na_xFePO_4 electrodes ($0 \le x \le 1$). For that, we use binary and mixed aqueous electrolyte solutions of constant ionic strength: 0.5 M$\{y\cdot[Li_2SO_4] + (1 - y)\cdot[Na_2SO_4]\}$ (with $0 \le y \le 1$). Analyzing the potential dependences of the intercalation charge, Q, the shifts in the resonance frequency, Δf_{exp}, and resonance width, $\Delta\Gamma$, EQCA offers a comprehensive description of the complex mechanism of ions insertion/extraction caused by a competition between the Li^+- and Na^+-ions. From a crystallographic point of view, both ions are expected to occupy the same intercalation sites in the host electrode. Although electrochemical delithiation of Li_xFePO_4 does not make sense as a practical means to produce Na-ions insertion type electrodes, the emphasis here is on the fundamental aspects of coinsertion of different ions from mixed electrolyte solutions and their coexistence in the electrode matrix. We report on extremely high Li-ion selectivity in mixed electrolyte solutions of Li^+- and Na^+-ions, providing unique information on the dynamics of the mechanical response of $FePO_4$ host to insertion/extraction of these ions.

2. EXPERIMENTAL SECTION

The quality and significance of the EQCA measurements strongly depend on the preparation of rigid composite electrode coatings. Recently, we have reported that conventional gas-assisted spraying of composite slurries of activated carbon powders yields reproducible and high-quality coatings.[11] This simple and efficient method has opened the door for a precise in situ monitoring of the ionic fluxes during capacitive charging of highly porous activated carbon electrodes used in electrochemical double-layer capacitors (EDLCs, also known as supercapacitors or ultracapacitors).

For the preparation of composite electrodes, we used commercially available carbon-coated $LiFePO_4$ powder. Scanning electron microscopy (SEM) images (Figure S1) show that the pristine powder consists of several hundred nanometer size ellipsoid-shape particles, and some larger agglomerates thereof (called here asperities). The BET specific surface area was 19 m^2/g, which is indicative of a particle size $\ll 1$ μm. The content of carbon was determined by elemental analysis to be 1.9 wt %. XRD patterns of pristine Li_xFePO_4 powder (Figure S2) showed an orthorhombic phospho-olivine type structure (space group no. 62 [*Pmna*], PDF file no. 01-081-1173). 10 wt % PVDF binder in *N*-methyl pyrrolidone was added to the slurry.

Gas-assisted spraying of the composite slurries onto the heated surface of 1 in. 5 MHz Maxtek crystals was used similarly to that described elsewhere.[11] A crucial point of the successful preparation of a composite coating is the rigidity, which is determined by the width of the resonance Γ measured in air. The following example of typical characteristics of the coated crystals measured by EQCA well illustrates the importance of the film rigidity. A clean Au-coated Maxtek crystal with a resonance frequency f = 4 986 169 Hz and a resonance width Γ = 36 Hz was used as the support for the electrode coating. After the crystal was coated with Li_xFePO_4 slurry and careful drying in vacuum, the resonance frequency decreased to f = 4 982 947 Hz. The observed shift of $\Delta f \approx 3.2$ kHz is due to the mass of the coating, whereas the resonance width in air increased only slightly, up to Γ = 46 Hz. In the solution, the typical values of $\Delta\Gamma$ are on the order of 100−200 Hz as demonstrated in Figures 2−4.

All EQCA measurements were carried out with the use of an E5100A High-Speed Network Analyzer in combination with a Schlumberger 1287 electrochemical interface driven by LabView 9.0 software. The latter was employed for data acquisition

dx.doi.org/10.1021/jp3117819 | J. Phys. Chem. C 2013, 117, 1247−1256

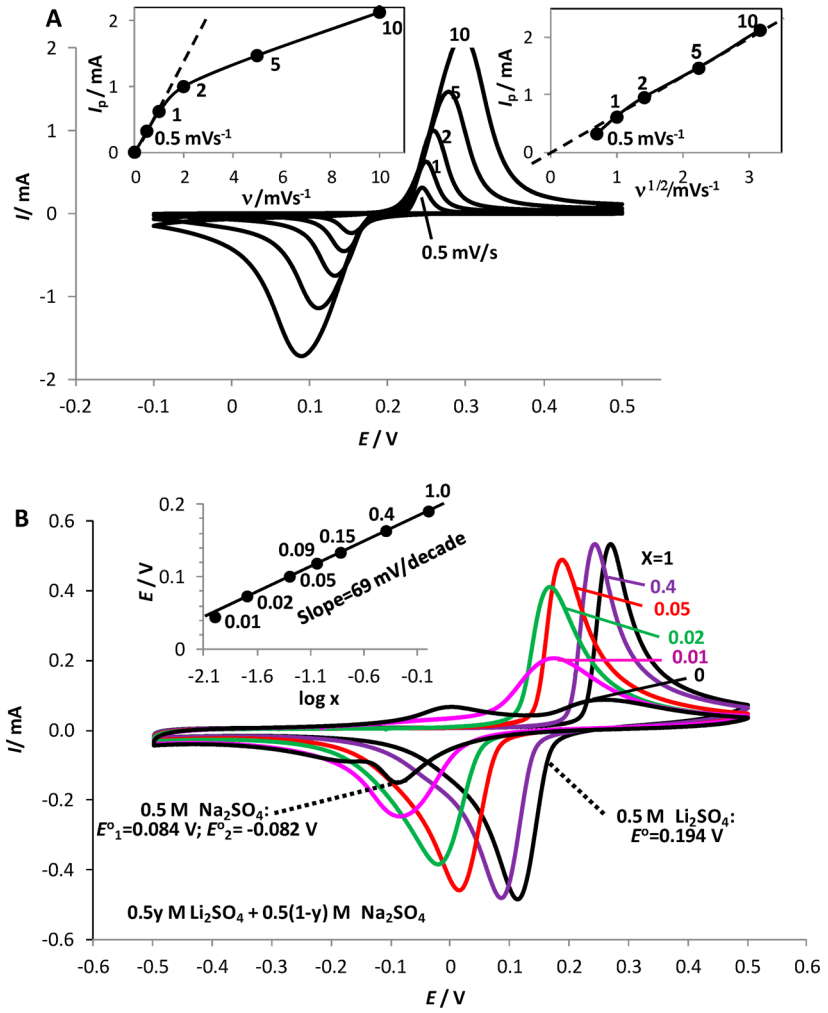

Figure 1. Cyclic voltammograms (CVs) for Li_xFePO_4-coated quartz crystal with a frequency shift in air of 3.6 kHz. (A) Cycling in neat aqueous 0.5 M Li_2SO_4 solution at various scan rates (insets in the left and right corners show the dependence of the peak height linearly with the scan rate and with the square-root of the scan rate, respectively). (B) Cycling in mixed electrolyte solutions with constant ionic strength, 0.5*y* M Li_2SO_4 + 0.5(1 − *y*) M Na_2SO_4, but containing Li^+ and Na^+ ions in different proportion as indicated. Inset in (B) represents the Nerstian relatioship between the formal redox potential E° of the $LiFePO_4/FePO_4$ couple taken as the middle-peak potentials of the anodic and cathodic CV peaks. The scan rate was 2 mV/s for all of the CVs measured.

and processing. During the measurements, the cells were kept at a constant temperature of 25.0 ± 0.2 °C. Other details on the experimental setup and the data processing were similar to those already reported.[9a,b] Electrochemical potentials were measured and reported versus a $Ag/AgCl/KCl_{(sat.)}$ reference electrode. In experiments with mixtures of Li_2SO_4 and Na_2SO_4, a $Hg/Hg_2SO_{4\ (sat.)}/0.5$ M Na_2SO_4 reference electrode was used: a constant potential difference −0.460 ± 0.001 V versus $Ag/AgCl/KCl_{(sat.)}$ was observed. For this reference, equilibrium was reached with respect to SO_4^{2-} anions in the electrolyte solution.

To convert the intercalation charge, *Q*, to the resonance frequency shift, Δf_{mass}, the mass of the inserted Li-ions ions, M_i, obtained from Faraday law was multiplied by the sensitivity of AT-cut quartz crystal at 25 °C (56.6 Hz cm^2/μg) via:

$$\Delta f_{mass} = -[(Q \cdot M_i)/(F \times 10^6)] \times 56.6$$

3. RESULTS AND DISCUSSION

Cyclic Voltammetry for Li_xFePO_4 Electrode in Binary and Mixed Li_2SO_4 + Na_2SO_4 Electrolyte Solutions. Figure 1A shows cyclic voltammograms (CVs) obtained with a $LiFePO_4$ electrode in a neat 0.5 M Li_2SO_4 solution. Although the height of the current peak initially increases with scan rate, ν, at the very beginning of the Li-ion insertion and extraction processes, the current does not depend appreciably on ν. This feature as well as the appearance of a characteristic bump on the voltage profile of the galvanostatic curve, sometimes called "overshoot of equilibrium voltage plateau"[12] (see inset in Figure 3), originate from two-phase character of the first-order phase transition during Li-ions insertion/extraction process.[12] The height of the CV peaks was plotted linearly and as the square-root of the potential scan rate, ν (see insets in Figure 1 in the left and right corners, respectively). It was found that at ν > 1 mV/s, the measured current is limited by diffusion, whereas for small scan rates (less than 1 mV/s), the square root dependence of current on the scan rate is transformed into a linear relationship. This strongly implies constancy of the intercalation charge, and this is well illustrated by Figure S3 showing saturation of both the intercalation charge and the resonance frequency shift of the electrode coating as the potential scan rate decreases (this experiment was performed with $LiFePO_4$-coated quartz crystal). For very slow rates of

dx.doi.org/10.1021/jp3117819 | J. Phys. Chem. C 2013, 117, 1247−1256

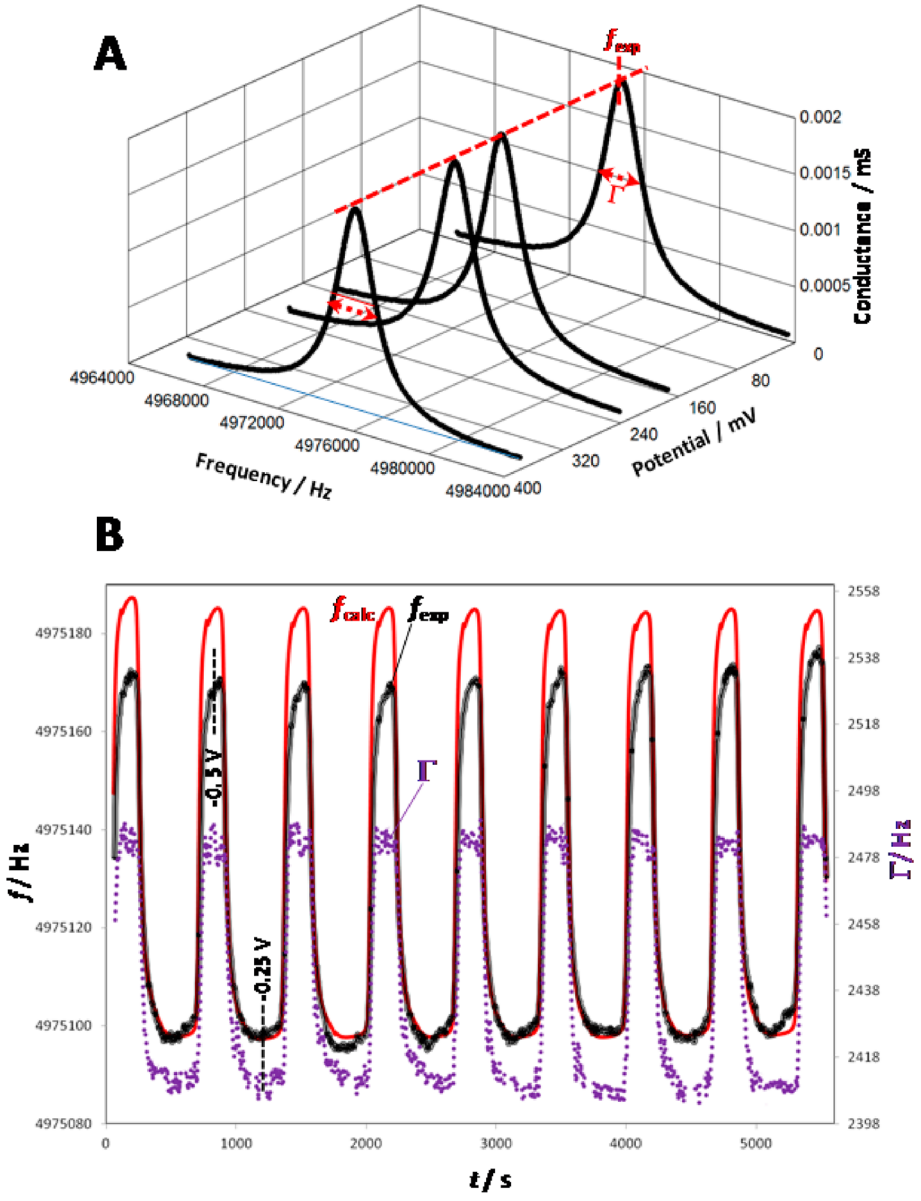

Figure 2. Raw quartz crystal admittance data: (A) resonance peaks measured at four different potentials for Li-ions extraction from a Li_xFePO_4-coated quartz crystal (the frequency shift in air due to electrode coating ~3.45 kHz), and (B) the periodic changes of the experimental and calculated (from the intercalation charge) resonance frequencies (f_{exp} and f_{calc}, respectively), and the resonance width Γ for the same coating continuously cycled in neat aqueous 0.5 M Li_2SO_4 solution between +0.4 and −0.25 V at a scan rate of 2 mV/s.

charge and discharge, the process of Li-ions insertion/extraction is believed to be kinetically controlled by a first-order phase transition, occurring relatively fast after initial nucleation and growth of the elements of the new phase in the bulk of the old one.[13]

Figure 1B shows CVs of Li_xFePO_4 obtained in mixed electrolyte solutions of Li and Na sulfates, in which the Li^+-to-Na^+ ratio ($\theta = y_{Li}{}^+/y_{Na}{}^+$) is changed by 2 orders of magnitude while keeping the ionic strength of the mixture constant. As the concentration of Li-ions in the solution decreases, the CV peaks shift gradually toward less positive potentials almost without a change in their shape in the range of sufficiently large values of θ. For smaller values of θ, the peak significantly broadens, shifting toward less positive potentials. Because this feature appears in the limit of small values of θ, this implies a kinetic limitation of the entire process due to slow diffusion of Li-ions in the solution. Ideally, one should expect that the formal redox potential of Li_xFePO_4 electrode (obtained from the CVs as the middle potential between their anodic and cathodic peaks) depends on y (Li^+-ions mole fraction in the mixture) with a slope of 59 mV per decade of y. This slope is typical for a reversible $1e^-$ (+ $1Li^+$-ion) ion insertion/extraction. By analogy with reversible redox reactions with surface-confined species (or distributed in a thin layer), this type of behavior can be identified as Nernstian. A slightly larger value of the slope (69 mV per decade) obtained in this experiment is most probably related to the activity of the potential-determining Li-ions in the concentrated solution, which deviates from their actual bulk concentrations. The Nernstian relationship between the Li_xFePO_4 peak potentials and the concentration of Li-ions in the solution does not contradict to (i) a much more narrow half-peak width like 23 mV at a scan rate of 0.5 mV/s as compared to 90 mV for a classical thin-layer Nernstian behavior, and (ii) a nonzero CV peak potential separation

dx.doi.org/10.1021/jp3117819 | J. Phys. Chem. C 2013, 117, 1247−1256

during charge and discharge, whereas zero peak-potential separation is typical for a classical Nernstian thin-layer behavior. Both of these features of the Li_xFePO_4 electrode are due to highly attractive short-range interactions of the intercalation species in the electrode bulk (up to first-order phase transition),[13c] which appear to be decoupled from the true equilibrium between Li-ions at the solid electrode/solution interface.

In neat Na_2SO_4 solution, Na^+-ions enter and leave the $FePO_4$ matrix via a two-step process with the formal redox potentials close to +0.084 and −0.082 V. These values are much lower than that for Li insertion from neat Li_2SO_4 solution (+0.194 V). The exceptionally high selectivity of Li-ions in the Li_xFePO_4 matrix with respect to Na-ions is not only seen from the slope of the electrode redox potential in mixed electrolyte solutions, but also from the lower anodic-to-cathodic peak potentials separation for Li-ion as compared to that for the Na-ion containing solution (Figure 1B). In addition, the Li-ion selectivity is also evidenced directly by EQCA. Figure S4B shows that Li_xFePO_4 in contact with a neat solution of Li_2SO_4 and in a mixed solution with prevailing Na-ions (molar fraction in the solution: $y = 0.015$) yields the same values for Δf_{exp} and $\Delta\Gamma$. The related CVs having similar shape shift toward less positive potentials on diminishing y in accordance with the Nernst law (Figure S4A). It is remarkable that even for a 20-times lower Li-concentration, there is still no shift of Δf_{exp} and $\Delta\Gamma$ (Figure S4B) as compared to the values for neat 0.5 M Li_2SO_4 solution. This is even more surprising becauase the corresponding CV became substantially broader (Figure S5A).

The selectivity of Li_xFePO_4 to Li-ions is explained as follows: During a negative potential scan from +0.5 V (corresponding to the pure, completely delithiated $FePO_4$ phase) toward −0.5 V, the Li-ions from the solution win the competition over Na-ions due to more favorable thermodynamics (higher redox potential) and fast kinetics. Finally, Li-ions occupy entirely a finite number of sites in the host matrix suitable for the ions accommodation even when Li-ions are present in a much smaller concentration in the solution than Na-ions.

The relative contribution of the thermodynamic and kinetic factors to the exceptionally high Li-ions selectivity can be revealed by the following estimation: When the molar fraction of Li-ions in the mixed solution is as low as $y = 0.05$, the electrode formal redox potential is about ∼0.110 V, which is slightly higher than the first redox potential of the electrode in neat Na_2SO_4 solution (∼0.084 V). This, again, is strongly indicative of the selectivity of $FePO_4$ electrode with respect to Li-ions insertion. We expect an even more pronounced competition between Li- and Na-ions at extremely low Li-to-Na ratios (θ) when the fast kinetics of Li-ions insertion can be confronted by the less favorable thermodynamics. In particular, a low redox potential for much diluted Li_2SO_4 solutions is believed to promote first Na-ions insertion into the electrode host. This considerably reduces the chance for Li-ions to be inserted into the host becauase Na-ions tend to become trapped in the host during a consecutive cycling of Li_xFePO_4 in neat Na_2SO_4 solution (Figure S6). The EQCA measurements reflect comprehensively the dynamic character of the mechanical response of $FePO_4$ to first (and subsequent) insertions and extractions of Na-ions as is discussed in more detail later (see also Figure 4).

EQCA of Li_xFePO_4 Electrode in Neat Li_2SO_4 Solution. Figure 2A shows raw resonance peaks measured with EQCA at four different potentials during Li-ion extraction from Li_xFePO_4. The peaks represent the frequency dependence of the real part of the crystal admittance (conductance), related to different electrode potentials. It is seen that the resonance frequency increases and the peaks become broader as the potential shifts toward more positive values. Figure 2B presents the EQCA data for the same continuously cycled electrode: The experimentally measured resonance frequency, f_{exp}, the resonance width, Γ, and the resonance frequency, f_{mass} were calculated from the simultaneously measured intercalation charge, Q, as a function of time. The latter is attributed to Li-ions rather than to electrolytic anions because Li_xFePO_4 is an ideal Li-ion exchanger (electrolytic anions cannot occupy sites in the electrode solid-state matrix). It is seen that the EQCA response shows a strongly correlated periodic variation of f_{exp}, f_{mass}, and Γ with time, and, thereby, with the applied potential that was varied linearly. The resonance width Γ is regarded in this work as a measure of the oscillation energy dissipation appearing during hydrodynamic interaction of the electrode particles/the entire composite coating with the contacting electrolyte solutions.

The potential dependence of $\Delta\Gamma$ can be qualitatively rationalized as follows: Initially, the pristine $LiFePO_4$ phase has a relaxed structure. During Li-ion extraction, the experimental resonance frequency increases with the injected charge, Q; the correlation factor between the Δf_{exp} and Δf_{mass} (the latter obtained from the value of Q) ranges between 0.8 and 0.9. Such an increase in the Δf_{exp} is accompanied by the increase in $\Delta\Gamma$ due to the distortion/deformation of the electrode particles/or entire coating, which modify the solid−liquid hydrodynamic interactions. The subsequent Li-ions insertion returns both Δf_{exp} and $\Delta\Gamma$ to their initial values characteristic of the initial relaxed state of the electrode host. The consecutive process of Li-ions insertion/extraction appeared to be chemically reversible.

As is detailed in the last section, the change in frequency due to the mass change during insertion/extraction process is subtracted from the value of Δf_{exp} with the rest assigned to the potential-dependent distortion of the composite electrode layer with the use of a hydrodynamic model. The following crystallographic information is essential for deeper understanding of the EQCA data obtained for $LiFePO_4$ electrode. The orthorhombic unit cell of phospho-olivine type consists of a distorted hexagonal close-packing of oxygen. In this structure, octahedrally coordinated Fe- and Li-ions and tetrahedrally coordinated P-ions are embedded. The experimental lattice parameters of $LiFePO_4$ were found to be $a = 10.3375$ Å, $b = 6.0112$ Å, and $c = 4.6950$ Å.[13a] During Li-ions extraction, the lattice constants a and b decrease by −5.6% and −4.3%, respectively, while c increases slightly by +1.3%.[14a] During Li^+ extraction and reinsertion, the olivine-type crystal structure is maintained, although the crystal structure undergoes geometric and volumetric changes.[14b] The migration of Li-ions takes place parallel to the b direction in tunnels between FeO_6 octahedra and PO_4 tetrahedra.[14c] Note that the potential-induced changes in the crystallographic cell volume of $LiFePO_4$ monocrystalline particles are the physical reason for the deformation/distortion of the composite electrode coating upon ions insertion/extraction. However, the link between both quantities is not direct in view of strong structural nonuniformity of the composite electrode coatings as is further discussed in the last section dedicated to admittance modeling.

EQCA of Li_xFePO_4 in Neat Li_2SO_4 Solution: Phase Transition Kinetics during a Slow Galvanostatic Charge

dx.doi.org/10.1021/jp3117819 | J. Phys. Chem. C 2013, 117, 1247−1256

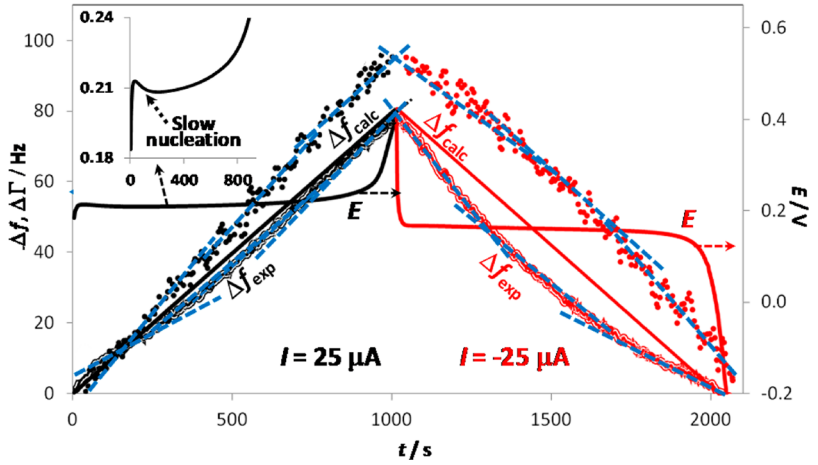

Figure 3. Galvanostatic charging of Li_xFePO_4-coated quartz crystal (the resonance frequency shift in air due to coating is 3.22 kHz, resonance width Γ = 41 Hz), and the related quartz crystal admittance components measured in situ in neat 0.5 M Li_2SO_4 solution. Single solid lines, triple solid lines, and solid dots relate to Δf_{mass}, Δf_{exp}, and ΔΓ, respectively, as indicated. The dashed blue lines show the different local slopes of Δf_{exp} and ΔΓ. The range of time with the overshoot on the voltage plateau due to slow nucleation and growth kinetics of Li-ions extraction is shown in the inset.

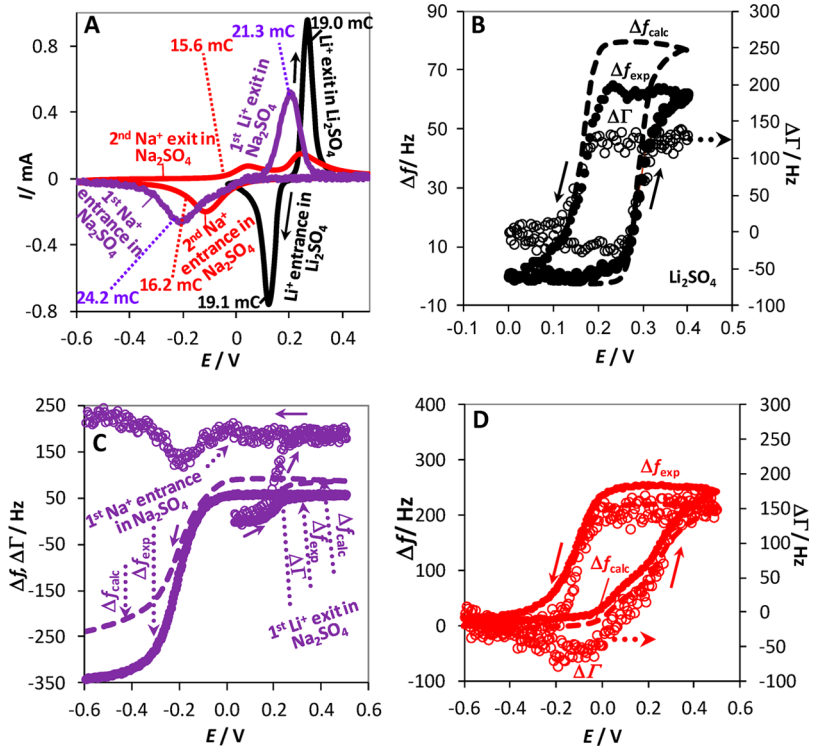

Figure 4. Cyclic voltammograms (panel A) for the Li_xFePO_4-coated quartz crystal (the resonance frequency shift in air 3.22 kHz, resonance width in air 41 Hz), measured simultaneously with the quartz crystal admittance components in different solutions (scan rate ν = 2 mV/s). The first charging process is carried out in neat 0.5 M Li_2SO_4 (black curves, panel B), then Li_xFePO_4-coated crystal was transferred to a neat 0.5 M Na_2SO_4 solution (violet curves in panel C). The second and the subsequent charge and discharge cycles in the 0.5 M Na_2SO_4 are performed with the crystal admittance components shown by red curves in panel D. The charges involved in the related Li- and Na-ions insertion/extraction are indicated in panel A. The EQCA components in panels B–D are shown by the same color as their related vis-à-vis CVs presented in panel A.

and Discharge. The galvanostatic testing during EQCA measurements allows studying the time dependence of Δf_{exp} and Δ Γ as a function of the intercalation charge *Q*. The latter is simply a linear function of time as a constant current is applied (see Figure 3). We now discuss the time dependences of all three quantities, Δf_{exp}, ΔΓ, and *Q*, for the half-cycle of Li-ion extraction. For the entire range of the applied potentials, Δf_{exp} was found to be very close to the linear plot of Δf_{mass} except for its middle part where the deviation is slightly larger. During the subsequent Li-ions insertion half-cycle, Δf_{exp} is close to Δf_{mass} only in the vicinity of both cutoff potentials. However, at the intermediate values of insertion, the discrepancy between the Δf_{exp} and Δf_{mass} is much larger than that for the Li-ions extraction half-cycle. The large discrepancy between the Δf_{exp} and Δf_{mass} for the Li-ions insertion has a clearly distinguished feature on the time-dependent plot of ΔΓ, when compared to the same plot for the Li-ions extraction half-cycle. It is well-known that the delithiated form of the solid-solution

dx.doi.org/10.1021/jp3117819 | J. Phys. Chem. C 2013, 117, 1247–1256

endmember (i.e., $FePO_4$) is characterized by structural deformation. On the basis of the local slopes of Δ Γ versus time plots, the deformation at the anodic cutoff potential seems to disappear upon the subsequent Li-ions insertion at a slower rate than it appears in the preceding Li-ions extraction half-cycle. This can be the origin of asymmetric charging/discharging of $LiFePO_4$ electrode. Also, this result is in accord with a similar asymmetric charge/discharge behavior of $LiFePO_4$ studied by in situ synchrotron X-ray diffraction and assigned to the delayed structural transformation of Li_xFePO_4.[15] In addition, the nucleation and growth feature that is observed at the beginning of Li-ions extraction is reflected by the reduced slope of the Δf_{exp} versus time curve and by the related large slope of the Δ Γ versus time plot (see Figure 3). This shows that EQCA is a powerful tool to provide in situ information on the dynamics of structural transformations. Advancing beyond the scope of qualitative description, quantitative aspects of the EQCA response during galvanostatic charge/discharge are discussed in the last section of this study.

Li_xFePO_4 in Mixed Solutions of Li and Na Sulfates: Selective Ions Insertion and Host Distortion. A special experiment was designed to probe the ion-exchange properties of Li_xFePO_4 including its mechanical response to foreign guest ions insertion. The electrode was first cycled repeatedly in neat Li_2SO_4 solution with the reproducible value of the charge during Li-ions insertion/extraction close to 19 mC. The black curves in Figure 4A and B show CVs and the EQCA components, respectively. The electrode, in the completely reduced state, then was thoroughly washed with deionized water and placed into a neat Na_2SO_4 solution. The first charge of Li_1FePO_4 and discharge of $FePO_4$ in Na-ion containing solution are shown by the blue curves in Figure 4A and C for the CVs and the EQCA components, respectively. This first charge showed a slightly higher value of the Li-ions extraction charge of 21.3 mC than that for continuously cycled electrode in Li_2SO_4 containing solution, most probably due to the effect of the first potential scan. The value of the charge due to first Na-ions was by 14% higher, 24.2 mC. This first charge/discharge in neat Na_2SO_4 solution was followed by the second charge/discharge in the same solution, which was qualitatively similar to all of the subsequent cycles (red curves in Figure 4A and D for the CVs and the EQCA components, respectively). The charge during the following (second) Na-ion extraction was considerably lower, 16.2 mC, followed by the charge during Na-ions insertion around 15.6 mC. The time dependences of Δf_{exp}, Δf_{mass}, and ΔΓ for the Li_xFePO_4 electrode cycled in neat Li_2SO_4 were highly reproducible: The electrode particles are distorted during Li-ions extraction followed by complete relaxation upon the subsequent Li-ions insertion.

Despite the fact that the amount of charge during the first Li-ion extraction from $LiFePO_4$ in neat Na_2SO_4 was similar to that for the Li-ion extraction in neat Li_2SO_4, the potential of the Li-ions release in Na_2SO_4 containing solution shifts toward less positive values in accordance with the Nernst equation, reflecting a drastic decrease of Li-ions concentration in the solution. The potential dependence of the EQCA components for these two systems was very close to each other.

First insertion of Na-ions into the completely delithiated $FePO_4$ host reflects clearly the conventional inertial mass loading contribution to the Δf_{exp} with only a slightly decreased value of Q as compared to that for the regular insertion of Li-ions from binary solutions. An additional, noninertial contribution to the Δf_{exp} appears as a result of the solid−liquid hydrodynamic interactions caused by a strong distortion of the $NaFePO_4$ matrix as it tries to accommodate the Na-ions, which are much larger than the pristine Li-ions.

The appearance of strong distortion in the $NaFePO_4$ matrix after first insertion of Na-ions into delithiated $FePO_4$ can be also expected from a comparison of the crystal unit cell parameters of $LiFePO_4$ and pure maricite ($NaFePO_4$). Maricite belongs to the same space group (*Pmna*) as the $LiFePO_4$ but has substantially larger lattice parameters: a = 8.990 Å, b = 6.862 Å, and c = 5.0470 Å.[16] Thus, the volume of the unit cell of $NaFePO_4$ is 311.3 $Å^3$ (as compared to 291.2 $Å^3$ for $LiFePO_4$).[14a] The mismatch between the reduced size of the channels in the $FePO_4$ phase and the size of Na-ions is probably responsible for a gradual trapping of Na-ions in the $FePO_4$ electrode during its continuous cycling (Figure S6).

The distortion of intercalation particles, and, thereby, in the entire electrode coating, can be traced through solid−liquid hydrodynamic interactions by a considerable increase of ΔΓ and the discrepancy between Δf_{exp} and Δf_{mass}. This remarkable ability of $FePO_4$ to relax during the second and subsequent insertion/extraction cycles of foreign guest ions is seen from a gradual decrease in growth of ΔΓ when sweeping the potential from 0.0 to −0.5 V. A comparison between the electrochemical and EQCA characteristics of $NaFePO_4/FePO_4$ and $LiFePO_4/FePO_4$ (Figure 4D and B, respectively) reveals a very similar increase in the value of ΔΓ (about 150 Hz) upon Na- and Li-ions extraction. The initial difference in the variation of the ΔΓ for these systems rapidly disappears upon the continuous cycling. This is related to the developed distortion of the electrode upon first Na-ions insertion between 0.0 and −0.5 V in contrast to the opposite trend for the $LiFePO_4/FePO_4$ system. Note that under the circumstance of a fairly comparable values for the width shift (ΔΓ) for the Na- and Li-ions insertion, the ratio of the related frequency shifts Δf_{exp} is close to 3 (i.e., mass loading contribution to Δf_{exp} prevails over the noninertial one under the specified conditions of charging).

Hydrodynamic Model of the Admittance of a Quartz Crystal Coated with a Composite Electrode Based on $LiFePO_4$ as the Active Mass. The characterization of composite Li-batteries electrodes during ions insertion/extraction is a new field of application for EQCA. The experimentally measured potential dependency of the admittance components, Δf_{exp} and ΔΓ, needs to be translated into geometric and porous structure parameters of the composite electrode. This can be done using a suitable hydrodynamic model describing the admittance of the electrode-coated oscillating quartz crystal in a liquid. Such a model accounting for a nonuniform character of the porous electrode layer has been reported recently.[9b] On the basis of the existence of smaller and larger size intercalation particles (see SEM images in Figure S1), the model considers individual agglomerates of primary particles (called asperities) and a pseudohomogeneous layer of smaller particles, which can also include usually small size carbon black particles (with carbon-coated $LiFePO_4$, we did not add carbon black at all). The PVdF binder is uniformly distributed throughout the entire composite electrode establishing its mechanical integrity. A sketch of a composite electrode based on the activated carbon or graphite particles is shown in Figure 1 in ref 9b; the same sketch is relevant for the composite $LiFePO_4$ electrode in this study. Our first assumption was that the intercalation particles were rigidly attached to the quartz crystal surface by the PVdF binder, which does not swell in

dx.doi.org/10.1021/jp3117819 | J. Phys. Chem. C 2013, 117, 1247−1256

aqueous solutions.[17] In ref 9b, we considered hydrodynamic interactions of as-described nonuniform (chemically and morphologically) composite electrode in a variety of liquids with different velocity decay length, δ.

The measurement of the admittance of the uncharged composite electrode coating prior to the analysis of the electrochemically induced changes in the electrode admittance in the solutions containing Li-salts is the indispensable initial stage of such an analysis. The goal is to characterize geometrically and morphologically the electrode coating prior to ions insertion. This cannot be done in a single liquid (e.g., in working solution at the initial value of OCV) because this solution has a single (fixed) velocity decay length, δ. We need for such a characterization a variety of liquids with different values of δ. The EQCA study of the electrode coating in a variety of liquids can be regarded as a kind of hydrodynamic spectroscopy of the electrode layer paying attention to the fact that the velocity decay length of the liquids, which is the only variable of the normalized frequency and resonance width responses (see eqs S1 and S2 in the Supporting Information and Figure 5), probes the electrode's structure in a way similar to that of the variable frequency probing the different relaxation stages of a complicated electrochemical process studied by conventional electrochemical impedance technique. We probe in the different liquids the porous electrode structure expressed in terms of two major parameters, the effective thickness of the coating, h, and its permeability length, ξ. The effect of the mass of the coating on the frequency shift has been subtracted from the measured experimental value. These parameters are found by a simultaneous fitting of the model with its explicit parameters of the porous and rough structure of the electrode to Δf_{exp} and $\Delta\Gamma$, determined experimentally in a variety of inert liquids, and characterize the initial geometric and porous structure of the electrode (see eqs S1 and S2 for Δf_{exp} and $\Delta\Gamma$, respectively). The result of this hydrodynamic test for the $LiFePO_4$ electrode coating is shown in Figure 5 with the evaluated initial (i.e., prior to the electrochemical test) parameters h_o and ξ_o.

We then further proceed with variation in the electrode potential during charging/discharging of the composite electrode changing the intercalation particles volume, which is traced by the admittance components Δf_{exp} and $\Delta\Gamma$ in the related EQCA measurements. It is important to note here that the pure mass change effect Δf_{mass} is subtracted from the measured frequency change, thus assigning the difference (together with the nonzero value of $\Delta\Gamma$) to the geometric and porous structure changes in the composite electrode layer. The potential-dependent changes of h and ξ (obtained by fitting $(\Delta f_{exp} - \Delta f_{mass})$ and $\Delta\Gamma$ with the hydrodynamic model; see eqs S1 and S2, respectively) constitute in our model two major global characteristics of the mechanical changes occurring in the porous composite electrode subjected to Li-ions extraction/reinsertion. As an example, Figure 6A and B shows the potential dependency of h and ξ obtained from the quartz crystal admittance measured in parallel with the galvanostatic curves showed in Figure 3. Both parameters increase and decrease by about 10% during full Li-ions extraction and insertion, respectively.

The potential-dependent variation of h and ξ for composite $LiFePO_4$ electrode is of value by itself (independent of its theoretical interpretation) as this relates directly to such practically important properties of Li-batteries electrode materials as integrity of the composite active mass used, its

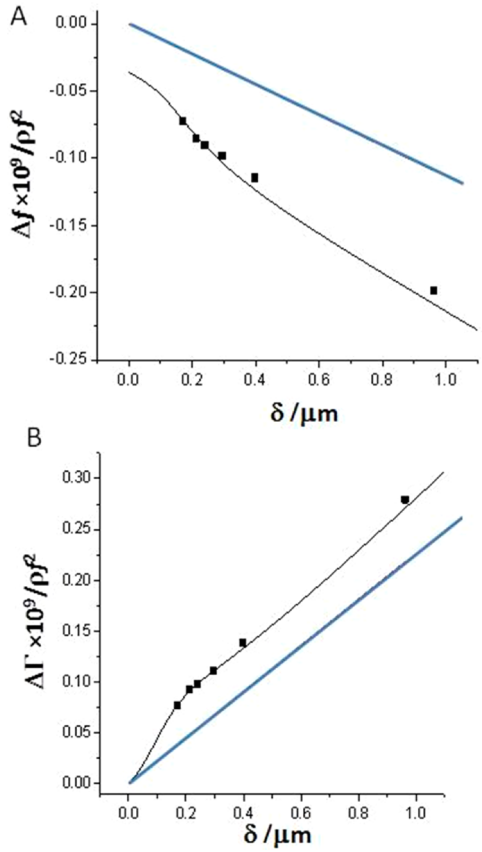

Figure 5. The dependence of the resonance frequency shift, $\Delta f/f^2\rho$ (A), and the resonance width, $\Delta\Gamma/f^2\rho$ (B), on the velocity decay length δ in different liquids for the $LiFePO_4$ composite electrode with frequency shift in air equal to 3.64 kHz. The points relate to the experimental data. The black lines are the result of calculations (eq S1). The straight blue lines are the responses of an ideally smooth interface. The parameters of fitting were as follows: ξ (the characteristic porous structure parameter of the PVdF sublayer) = 0.2 μm; L (the characteristic thickness of the PVdF sublayer) = 0.42 μm; n (the occupation density) = 0.0021 μm^{-2}; R (the roughness coefficient of the PVdF sublayer) = 1.1; and r (radius of bumps) = 3.3 μm.

electronic and ionic conductivity, depth of charge and discharge (including active mass utilization), and, finally, the factors affecting batteries long-term cyclability. Next, despite the fact that the mass effect was subtracted from the experimental frequency change, there should be a correlation between the changes of h and ξ observed and the amount of the intercalation charge so that the time dependence of these parameters in comparison with that of the intercalation charge should provide indirect information on the effect of ions insertion/extraction on the mechanical status of the electrode host matrix.

In the description of a possible theoretical interpretation of the experimental parameters Δf_{exp} and $\Delta\Gamma$ via the parameters h and ξ, we noted only briefly that PVdF binder shows a rigid mechanical behavior in aqueous solutions. Having in mind that Li-ion extraction from $LiFePO_4$ results in approximately 7% of the intercalation particles volume decrease, it seems that the increase in the calculated value of ξ is what is intuitively expected. The simultaneous increase in h is to some extent counterintuitive in view of the decrease of the deintercalated particles volume. A possible explanation is that the mechanical

dx.doi.org/10.1021/jp3117819 | J. Phys. Chem. C 2013, 117, 1247−1256

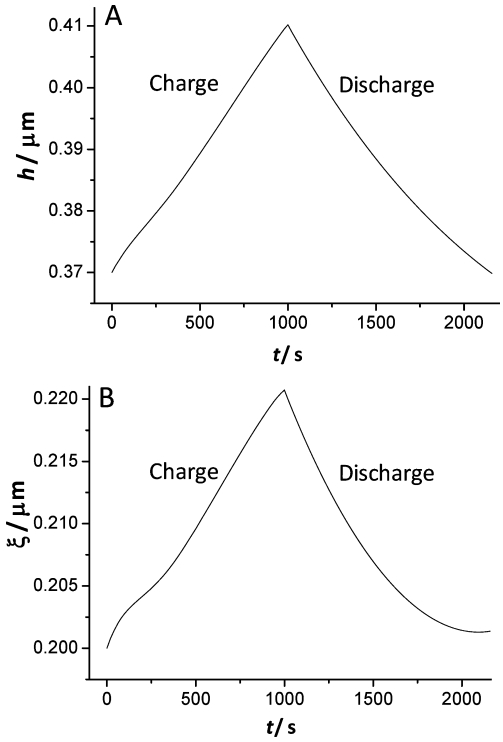

Figure 6. Final geometric and porous structure parameters, h (A) and ξ (B), found for the composite $LiFePO_4$ electrode coating cycled galvanostatically (see Figure 3). These parameters were found by fitting the experimental changes of the components of the admittance, ($\Delta f_{exp} - \Delta f_{mass}$) and $\Delta\Gamma$ (see Figure 3), to eqs S1 and S2, respectively. Initial values of these parameters are those found by the hydrodynamic spectroscopy characterization of this composite electrode (see Figure 5).

properties of the composite electrode, in particular the ability to deform, cannot be presented simplistically as a sum of the changes experienced by the individual intercalation particles. Note that the electrical properties of a composite electrode can be reduced to the properties of the constituent intercalation particles in a particular case when both electronic conductance of the active mass and the ionic conductance of the electrolyte in the electrode's pores are infinitely high. Nonequivalence of the mechanical properties of the composite electrode with that of the individual particles stems from the fact that the mechanical attachment of the binder to the intercalation particles may fully or only partially allow them to deform, making the resultant deformation highly nonuniform. This is known as the problem of free and clamped surfaces in the development of elastic deformations of host electrodes caused by ions insertion/extraction.[18] It is reasonable to assume that keeping the same binder but selecting another solvent causing a stronger swelling may increase the ratio of free-to-clamped surfaces ratio in the composite electrode. Thus, we performed EQCA experiments with composite $LiFePO_4$ electrodes containing the same amount of PVdF as previously, for cycling the electrode in the aqueous solution, but this time replacing the aqueous solution with 1 M $LiPF_6$/EC:DMC (1:1). The latter now represents a standard electrolyte solution used in commercial Li-ion batteries. Figure S7A shows that the galvaniostatic curve in this nonaqueous electrolyte solution is very similar to that found in the aqueous solution of Li_2SO_4 (Figure 3). From the related raw values of Δf_{exp} and $\Delta\Gamma$, we calculated the parameters h and ξ (Figure S7B and C, respectively). It is seen that h demonstrates first a small increase at the beginning of Li-ions extraction followed by a large decrease as Li-ions extraction proceeds further (the change in the parameter ξ is also modified with respect to that found in aqueous solutions; compare Figure S7C and S7B). PVdF partially swells in highly polar aprotic solvents,[19] implying that the swollen binder allowed for more complete potential induced deformation of the intercalation particles (dictating the decrease in volume of deintercalated electrode). We can suggest that the swelled binder increases the ratio of free-to-clamped surfaces of intercalation particles in the composite electrode. In this case, mechanical properties of the porous nonuniform intercalation electrode are closer to the properties of the individual intercalation particles as compared to the case of the absolutely rigid binder. It is thus clear that EQCA studies may provide exceptionally important information on the mechanical behavior of binders for their effective use in composite Li-batteries electrodes, also for deeper understanding of their role during batteries cycling.

4. CONCLUSIONS

Exceptionally high selectivity of Li-ions insertion into $FePO_4$ as compared to that of Na-ions was found in mixed aqueous electrolyte solutions of lithium and sodium sulfates. The concentration dependence of the electrode redox potential is in accord with the Nernst law. The selectivity effect is of a mixed kinetic and thermodynamic origin. For the latter, we need to consider that the formal redox potential of $LiFePO_4/Li^+$ couple is much more positive than that for Na^+-ion. To the best of our knowledge, testing the ionic selectivity of the intercalation-type electrodes in mixed liquid solutions has never been earlier reported. The only exception is a very specific 3D Chevrel phase, which has been shown to exhibit high ion insertion selectivity for the cations of different size.[20] The EQCA methodology applied to the composite electrode coatings allowed us to demonstrate a highly reversible and reproducible variation of the resonance frequency, Δf_{exp}, and the resonance width, $\Delta\Gamma$, with applied potential upon continuous Li-ions insertion/extraction cycles. The novel dynamic features of the mechanical response of the Li_xFePO_4 host to foreign guest ions insertion (Na^+- versus Li^+-ions) have been described qualitatively. The EQCA method probes ion insertion/extraction-induced changes of the mechanical properties of the composite electrodes indirectly, via variation of the solid–liquid interactions, traced by two major parameters, Δf_{exp} and $\Delta\Gamma$. The interactions themselves are modified due to the distortion/deformations of the intercalation particles and, via the polymeric binder used, of the entire composite electrode upon ions insertion/extraction. Using the model of a nonuniform composite electrode laid on the surface of oscillating quartz crystal interacting hydrodynamically with the contacting solution, we have translated the experimental EQCA components, Δf_{exp} and $\Delta\Gamma$, into the related variation of the electrode coating thickness, h, and its effective permeability, ξ.[9c] The EQCA methodology may have surprising implications in very hot topics of present and future LIB research on the role of potential-induced stress–strain relationship, referred to both individual intercalation particles, and the entire chemically and topographically nonhomogeneous composite electrode coating including the nature of polymeric binders, in determining the capacity and cycling life of the electrodes for LIB and carbon supercapacitor devices.

dx.doi.org/10.1021/jp3117819 | J. Phys. Chem. C 2013, 117, 1247–1256

■ ASSOCIATED CONTENT

Supporting Information

SEM and XRD characterization. This material is available free of charge via the Internet at http://pubs.acs.org.

■ AUTHOR INFORMATION

Corresponding Author

*E-mail: levimi@mail.biu.ac.il (M.D.L.); aurbach@mail.biu.ac.il (D.A.).

Notes

The authors declare no competing financial interest.

■ ACKNOWLEDGMENTS

V.P. acknowledges funding from the German Federal Ministry for Research and Education (BMBF) in support of the nanoEES3D project (award number 03EK3013) as part of the strategic funding initiative energy storage framework. V.P. also thanks Prof. Eduard Arzt for his continuing support.

■ REFERENCES

(1) (a) Padhi, A. K.; Nanjundaswamy, K. S.; Goodenough, J. B. *J. Electrochem. Soc.* **1997**, *144*, 1188−1194. (b) Delmas, C.; Maccario, M.; Groguennec, L.; Le Cras, F.; Weill, F. *Nat. Mater.* **2008**, *7*, 665−671.

(2) (a) Meethong, N.; Huang, H.-Y. S.; Carter, W. C.; Chiang, Y. M. *Electrochem. Solid-State Lett.* **2007**, *10*, A134−A138. (b) Zhu, Y.; Wang, C. *J. Phys. Chem. C* **2010**, *114*, 2830−2841.

(3) Deshpande, R.; Cheng, Y.-T.; Verbrugge, M. W. *J. Power Sources* **2010**, *195*, 5081−5088.

(4) (a) Pyun, S.-I.; Go, J.-Y.; Shin, H.-C. *J. New Mater. Electrochem. Syst.* **2002**, *5*, 143−148. (b) Go, J.-Y.; Pyun, S.-I. *J. Electrochem. Soc.* **2003**, *150*, A1037−A1043.

(5) (a) Chung, K. Y.; Kim, K.-B. *J. Electrochem. Soc.* **2002**, *149*, A79−A85. (b) Chason, E.; Sheldon, B. W. *Surf. Eng.* **2003**, *19*, 387−391. (c) Soni, S. K.; Sheldon, B. W.; Xiao, X.; Tokranov, A. *Scr. Mater.* **2011**, *64*, 307−310. (d) Mukhopadhyay, A.; Tokranov, A.; Sena, K.; Xiao, X.; Sheldon, B. W. *Carbon* **2011**, *49*, 2742−2749. (e) Sethuramana, V. A.; Van Winkle, N.; Abraham, D. P.; Bower, A. F.; Guduru, P. R. *J. Power Sources* **2012**, *206*, 334.

(6) (a) Noel, M. A.; Topart, P. A. *Anal. Chem.* **1994**, *66*, 484−491. (b) Josse, F.; Cernosek, R. W. Resonant Piezoelectric Devices as Physical and Biochemical Sensors. *Smart Sensors and MEMS. NATO Science Series II: Mathematics, Physics and Chemistry*; Kluwer Academic Publishers: Dordrecht, Boston, London, 2004; Vol. *181*, pp 91−123. (c) Arnau, A., Ed. *Piezoelectric Transducers and Applications*; Springer-Verlag: Berlin, Heidelberg, 2008.

(7) (a) Buttry, D. A.; Ward, M. D. *Chem. Rev.* **1992**, *92*, 1355−1379. (b) Bruckenstein, S.; Shay, M. *Electrochim. Acta* **1985**, *30*, 1295−1300. (c) Bandey, H. L.; Hillman, A. R.; Brown, M. J.; Martin, S. J. *Faraday Discuss.* **1997**, *107*, 105−121. (d) Hillman, A. R. *J. Solid State Electrochem.* **2011**, *15*, 1647−1660. (e) Kanazawa, K. K.; Gordon, J. G., II. *Anal. Chim. Acta* **1985**, *175*, 99−105. (f) Johannsmann, D. *Phys. Chem. Chem. Phys.* **2008**, *10*, 4516−4534. (g) Tsionsky, V.; Daikhin, L.; Urbakh, M.; Gileadi, E. In *Electroanalytical Chem. A Series of Advances*; Bard, A. J., Rubinstein, I., Eds.; Marcel Dekker: New York, 2004; Vol. *22*, pp 2−102.

(8) (a) Hillman, A. R.; Efimov, I.; Ryder, K. S. *J. Am. Chem. Soc.* **2005**, *127*, 16611−16620. (b) Takayuki, U.; Matsuhiko, N.; Takashi, I.; Isamu, U. *J. Electrochem. Soc.* **2000**, *147*, 2057−2060. (c) Dong, S.; Chung, K. Y.; Cho, W. I.; Kim, K. B. *J. Power Sources* **2003**, *114*, 253−263.

(9) (a) Daikhin, L.; Gileadi, E.; Katz, G.; Tsionsky, V.; Urbakh, M.; Zagidulin, D. *Anal. Chem.* **2002**, *74*, 554−561. (b) Daikhin, L.; Levi, M. D.; Sigalov, S.; Salitra, G.; Aurbach, D. *Anal. Chem.* **2011**, *83*, 9614−9621. (c) Daikhin, L.; Urbakh, M. *Langmuir* **1996**, *12*, 6354−6360. (d) Winter, M.; Wrodnigg, G. H.; Besenhard, J. O.; Biberacher, W.; Novak, P. *J. Electrochem. Soc.* **2000**, *147*, 2427−2431.

(10) (a) Moreau, P.; Guyomard, D.; Gaibicher, J. *Chem. Mater.* **2010**, *22*, 4126−4128. (b) Ellis, B. L.; Makahnouk, W. R. M.; Makimura, Y.; Toghill, K.; Nazar, L. F. *Nat. Mater.* **2007**, *6*, 749−753. (c) Kim, S.-W.; Seo, D.-H.; Ma, X.; Ceder; Kang, K. *Adv. Energy Mater.* **2012**, *2*, 710−721.

(11) (a) Levi, M. D.; Salitra, G.; Levy, N.; Aurbach, D.; Maier, J. *Nat. Mater.* **2009**, *8*, 872−875. (b) Levi, M. D.; Levy, N.; Sigalov, S.; Salitra, G.; Aurbach, D.; Maier, J. *J. Am. Chem. Soc.* **2010**, *132*, 13220−13222.

(12) Bai, P.; Cogswell, D. A.; Bazant, M. Z. *Nano Lett.* **2011**, *11*, 4890−4896.

(13) (a) Allen, J. L.; Jow, T. R.; Wolfenstine, J. *Chem. Mater.* **2007**, *19*, 2108. (b) Oyama, G.; Yamada, Y.; Natsui, R.-i.; Nishimura, S.-i.; Yamada, A. *J. Phys. Chem. C* **2012**, *116*, 7306−7311. (c) Levi, M. D.; Aurbach, D. *J. Solid State Electrochem.* **2007**, *11*, 1031−1042.

(14) (a) Andersson, A. S.; Thomas, J. O. *J. Power Sources* **2001**, *97*−*98*, 498−502. (b) Malik, R.; Zhou, F.; Ceder, G. *Nat. Mater.* **2011**, *17*, 587−590. (c) Morgan, D.; Van der Ven, A.; Ceder, G. *Electrochem. Solid-State Lett.* **2004**, *7*, A30−A32.

(15) Chang, H.-H.; Chang, C.-C.; Wu, H.-C.; Yang, M.-H. *Electrochem. Commun.* **2008**, *10*, 335−339.

(16) Bridson, J. N.; Quinlan, S. E.; Tremaine, P. R. *Chem. Mater.* **1998**, *10*, 763−768.

(17) Bottino, A.; Capannelli, G.; Munari, S.; Turturro, A. *J. Polym. Sci., Part B: Polym. Phys.* **1988**, *26*, 785−794.

(18) McKinnon, W. R.; Haering, R. R. Physical Mechanisms of Intercalation. In *Modern Aspects of Electrochemistry*; White, R. E., Bockris, J. O. M., Conway, B. E., Eds.; Plenum Press: New York, 1983; Vol. *15*, pp 235−303.

(19) Kynar PVDF. Resins for Battery Manufacture (www.kynar.com); Arkema Inc.: Market Street, Philadelphia, PA, 2000.

(20) (a) Seghir, S.; Boulanger, C.; Diliberto, S.; Lecuire, J.-M.; Potel, M.; Merdrignac-Conanec, O. *Electrochem. Commun.* **2008**, *10*, 1505−1508. (b) Seghir, S.; Boulanger, C.; Diliberto, S.; Lecuire, J.-M.; Bouquet, V.; Potel, M.; Guilloux-Viry, M. *Electrochem. Commun.* **2010**, *12*, 1734−1737.